GSA DATA REPOSITORY 2014186

The contribution of mountains to global denudation

Isaac J. Larsen*, David R. Montgomery, and Harvey M. Greenberg

DATA SOURCES

The soil total and chemical denudation rate data in Fig. 1a are compiled from Riebe et al. (2004); Burke et al. (2007); Burke et al. (2009); Dixon et al. (2009); Norton and von Blanckenburg (2010); Dixon et al. (2012); Ferrier et al. (2012); and Larsen et al. (2014). The data are as originally published, except some of those from Riebe et al. (2004), which have been re-calculated using chemical erosion factors reported by Riebe and Granger (2013). The catchment sediment and solute yield data are for 299 ocean-draining rivers from Milliman and Farnsworth (2011). Pre-dam data were used when these data were reported. Data from five rivers (Colorado, Haihe, Rhine, Patuxent, and Severn) in the database were excluded from the statistical analyses due to high anthropogenic influence on either chemical or physical denudation; though most rivers in the database likely are influenced by humans to varying degrees. Removal of these data resulted in an increase in the chemical-physical denudation R^2 value, but had very little influence on the power-law scaling exponent. Only 265 of the 299 catchments were used to generate Fig. 4 because we could not delineate catchment areas that were consistent with those reported in Milliman and Farnsworth (2011) for 34 catchments; see p. 7 of Milliman and Farnsworth (2011) for a note regarding catchment areas. The mean ratio of catchment area reported by Milliman and Farnsworth (2011) to the catchment area we determined for the 265 catchments was 1.0 and the standard deviation was 0.2. We used the catchment area and unit area yield data reported by Milliman and Farnsworth (2011) to generate Figure 4, rather than re-calculating yields based on the areas we estimated.

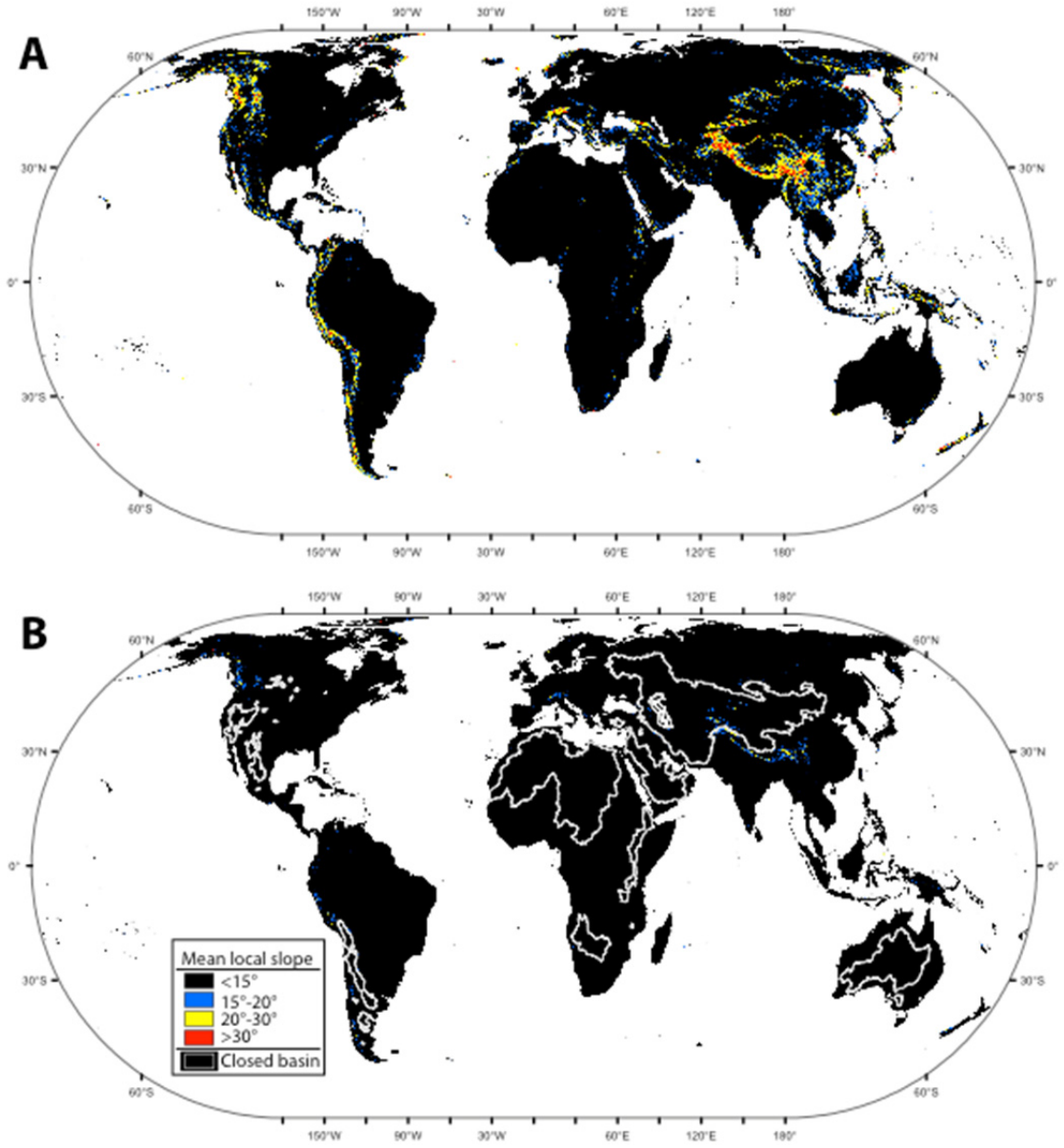

Figure DR1. Maps of mean local slope for the: A) 3 arc-second DEM and B) 30 arc-second DEM. Closed basins are outlined in B. Slope angles were calculated by accounting for the latitudinal dependence on grid cell shape caused by the pole-ward convergence of meridians (Horn, 1981) using separate algorithms for elevation grids that spanned 1° of latitude. The 1°-spanning slope grids were then combined to generate a global slope map.

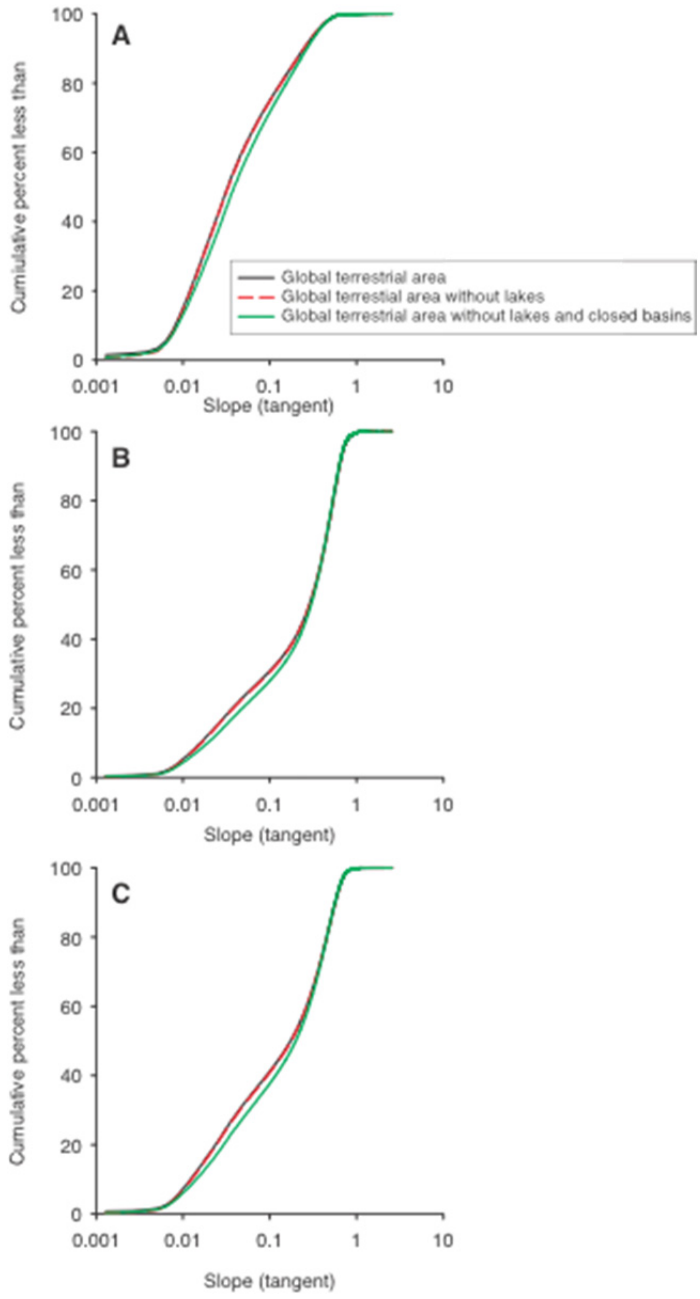

Figure DR2. Global distributions of: A) mean local slope; B) total denudation; and C) chemical denudation for Earth's terrestrial surface, the terrestrial surface without lakes, and the terrestrial surface without lakes or closed basins. The lake data are from the *WWF Global Lakes and Wetlands Database*: http://worldwildlife.org/pages/global-lakes-and-wetlands-database and the FAO closed basins data are from the *World map of the major hydrological basins (Derived from HydroSHEDS)* dataset: http://www.fao.org/geonetwork/srv/en/metadata.show?id=38047

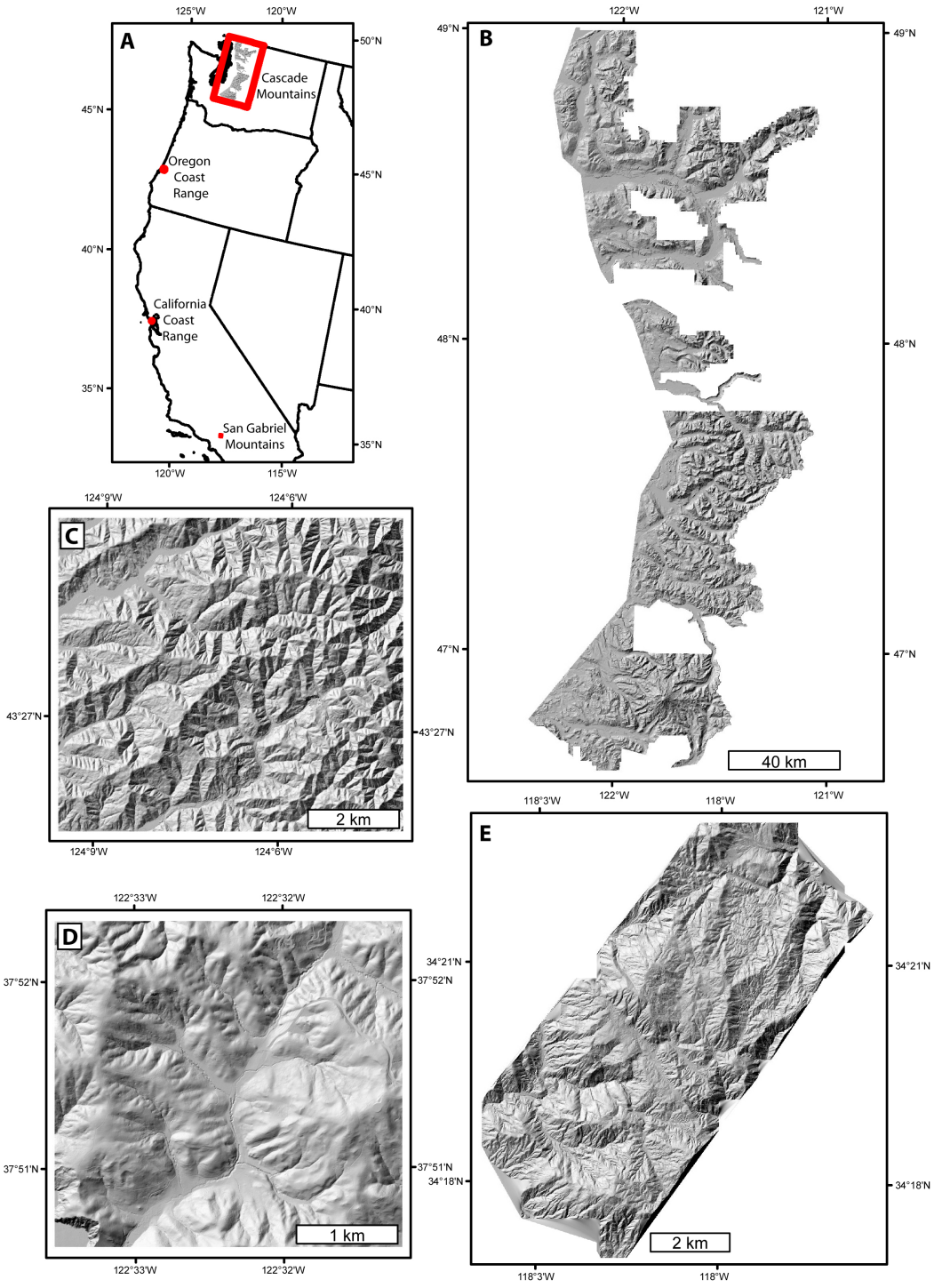

Figure DR3. A) Map showing the location and spatial extent of each LiDAR dataset for B) the Cascade Mountains (12122 km^2), C) Oregon Coast Range (418 km^2), including Mettman Ridge, D) California Coast Range (11 km^2), including Tennessee Valley, and E) the San Gabriel Mountains (57 km^2).

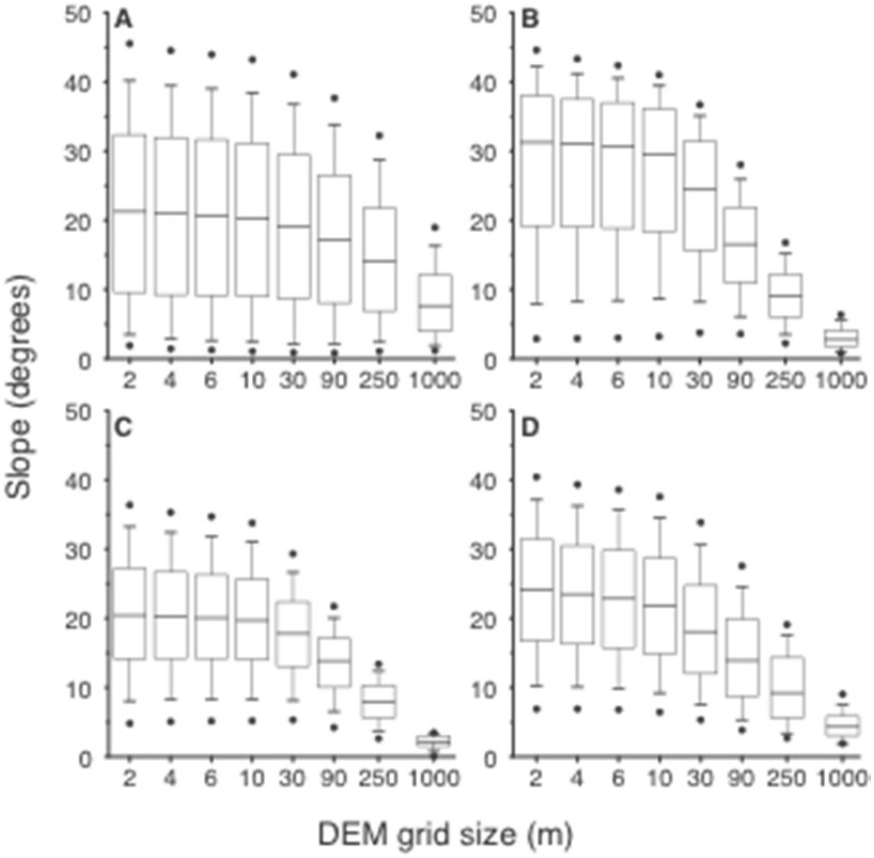

Figure DR4. Box-plots showing slope angle distributions as a function of different DEM grid cell sizes for sites in the A) Cascade Mountains, B) Oregon Coast Range, C) California Coast Range, and D) San Gabriel Mountains. The horizontal line is the median, the box spans the inter-quartile range, lines span the 10^{th} and 90^{th} percentiles, and the circles denote the 5^{th} and 95^{th} percentiles.

REFERENCES CITED

Burke, B., Heimsath, A. and White, A.. 2007, Coupling chemical weathering with soil production across soil-mantled landscapes: Earth Surface Processes and Landforms, v. 32, p. 853-873.

Burke, B., Heimsath, A., Dixon, J., Chappell, J. and Yoo, K., 2009, Weathering the escarpment: chemical and physical rates and processes, south-eastern Australia. Earth Surface Processes and Landforms, v. 34, p. 768-785.

Dixon, J., Heimsath, A. and Amundson, R., 2009, The critical role of climate and saprolite weathering in landscape evolution:. Earth Surface Processes and Landforms, v. 34, p. 1507-1521.

Dixon, J., Hartshorn, A., Heimsath, A., DiBiase, R. and Whipple, K., 2012, Chemical weathering response to tectonic forcing: A soils perspective from the San Gabriel Mountains, California. Earth and Planetary Science Letters, v. 323-324, p. 40-49.

Ferrier, K., Kirchner, J. W. and Finkel, R., 2012, Weak influences of climate and mineral supply rates on chemical erosion rates: Measurements along two altitudinal transects in the Idaho Batholith: Journal of Geophysical Research 117, F02026 (2012).

Horn, B.K.P., 1981, Hill shading and the reflectance map: Proceedings of the IEEE, v. 69, p. 14-47, doi:10.1109/PROC.1981.11918.

Larsen, I. J., Almond, P. C., Eger, A., Stone, J. O., Montgomery, D. R., and Malcolm, B., 2014, Rapid mountain weathering breaks global speed limit, Science, v. 343, p. 637-640.

Milliman, J., and Farnsworth, K., 2011, River Discharge to the Coastal Ocean: A Global Synthesis: New York, Cambridge University Press, 384 p.

Norton, K. and von Blanckenburg, F., 2010, Silicate weathering of soil-mantled slopes in an active Alpine landscape: Geochim. Cosmochim. Acta, v. 74, p. 5243-5258.

Riebe, C. S., Kirchner, J. W. and Finkel, R. C., 2004, Erosional and climatic effects on long-term chemical weathering rates in granitic landscapes spanning diverse climate regimes: Earth and Planetary Science Letters: v. 224, p. 547-562.

Riebe, C. S. and Granger, D. E., 2013, Quantifying effects of deep and near-surface chemical erosion on cosmogenic nuclides in soils, saprolite, and sediment: Earth Surface Processes and Landforms, v. 38, p. 523-533.